Received: 5 November 2021 | Revised: 27 December 2021 | Accepted: 31 December 2021

DOI: 10.1002/mmce.23076

ORIGINAL ARTICLE

INTERNATIONAL JOURNAL OF RF AND MICROWAVE COMPUTER-AIDED ENGINEERING WILEY

# Synthesis of lumped-element dual-band bandpass filters with independently controllable bandwidth

**Zhuoyin Chen** | **Yongle Wu** | **Weimin Wang**

School of Electronic Engineering, Beijing Key Laboratory of Work Safety Intelligent Monitoring, Beijing University of Posts and Telecommunications, Beijing, China

**Correspondence**
Yongle Wu, School of Electronic Engineering, Beijing Key Laboratory of Work Safety Intelligent Monitoring, Beijing University of Posts and Telecommunications, P.O. Box 282, Beijing 100876, China.
Email: wuyongle138@gmail.com

**Funding information**
National Natural Science Foundations of China, Grant/Award Numbers: National Natural Science Foundations of China, U20A20203, U21A20510, 61971052; Fundamental Research Funds for the Central Universities, Grant/Award Number: 2021XD-A07-1; Key Research and Development Project of Guangdong Province, Grant/Award Number: 2020B0101080001

**Abstract**

In this article, a novel synthesis method for lumped-element dual-band bandpass filters (DBPFs) with independently controllable bandwidth is proposed. The proposed lumped-element DBPF exhibits the advantages including two passbands with independently controllable bandwidth, arbitrary frequency ratio, availability for different lowpass prototypes, and compact size below 6 GHz. This design theory is based on the equivalents of dual-band J-inverters and LC resonators which combines generalized dual-band resonators theory with independently controllable bandwidth. A dual-band bandpass frequency transformation and four circuit conversions are derived. For demonstration, three cases of DBPF with different bandwidths, frequency ratios, and orders are designed, fabricated, and measured. The simulated and measured results have a good agreement, validating the proposed synthesis theory.

**KEYWORDS**

dual-band filter, frequency transformation, independently controllable bandwidths, lumped elements, printed circuit board

## 1 | INTRODUCTION

With the rapid development of wireless communication systems, various research has concentrated on the dual-band bandpass filters (DBPFs)[1–13] to use for multi-frequency channels and saving board size, which can be used for other devices, such as dual-band impedance transformers[14] and dual-band power dividers.[15]

The most basic method to design a DBPF is parallel connecting two bandpass filters or cascading a bandstop filter and a wideband bandpass filter.[1] However, these methods need to require impedance matching and occupy a large area. Using the frequency transformation method is more commonly used. In Reference 2, a symmetric DBPF synthesis method based on lumped elements is presented. In Reference 3, a design method for DBPF with different bandwidths is realized by frequency transformation. In Reference 4, a synthesis method for DBPF is proposed, which is using two lowpass prototypes based on coupling matrix. Instead, a dual wideband BPF is realized by frequency mapping in Reference 5.

The DBPF circuit can be implemented using distributed components,[1–8] lumped components,[9–11] or hybrid components.[12,13] Circuit size and complexity can be reduced by using lumped or hybrid components, especially at low frequencies (below 6 GHz). In Reference 9, a lumped-element dual-band coplanar waveguide filter using impedance matching is proposed. This method can realize independently controllable bandwidth using the quarter-wavelength transmission line inverter. In Reference 10, a synthesis method for lumped DBPF with independently controllable bandwidth by adopting capacitive networks as dual-mode J-inverters is presented. However, the design methods of lumped-element DBPF with independently controllable bandwidth proposed in References 9,10 are

  

complex. Based on frequency transformation in Reference 2, a synthesis method of DBPF with circuit conversion is proposed in Reference 12. This method can realize a wide fractional bandwidth range and wide center frequency ratio using hybrid components. However, the two passbands proposed in Reference 12 cannot be tuned independently because all the passbands are derived from the same lowpass prototype. In Reference 15, a design method of dual-band unequal filtering power divider is presented. This method can design DBPFs with arbitrary frequency ratios and independently controllable bandwidth based on microstrip lines, but the design procedure is complicated and the designed circuit occupies a large area.

In this article, based on dual-band bandpass frequency transformation and circuit conversions, a novel synthesis method of lumped-element ICBW DBPF is proposed. Base on the equivalents of dual-band J-inverters and LC resonators, the lowpass prototype to dual-band bandpass transformation with independently controllable bandwidth was derived. Simultaneously, four type circuit equivalent conversions were used to simplify the circuit for implementation. Compared to References 9,10, extra matching networks are not required. Overall, the proposed LC DBPF has the following significant advantages: (i) independently controllable bandwidth between two passbands; (ii) arbitrary frequency ratios; (iii) compact size below 6 GHz; (iv) large range of fractional bandwidth; (v) availability for different lowpass prototypes.

## 2 | SYNTHESIS THEORY OF THE PROPOSED DUAL-BAND BPF

A generalized DBPF can consist of dual-band admittance inverters (DBAIs) and dual-band resonators (DBRs). The generalized DBRs with independently controllable bandwidth can be expressed as Reference 15.

$$Y_B(\omega_1) = Y_B(\omega_2) = 0, \tag{1}$$

$$b_{\omega_r} = \frac{\omega_r}{2}\frac{\partial}{\partial\omega}\mathrm{Im}[Y_B(\omega)]\Big|_{r=1,2}, \tag{2}$$

$$b_{i\omega_r} = \frac{g_i}{FBW_r R_S}, i = 2,3,\ldots,N-1, \tag{3}$$

where $Y_B$ is the input admittance of DBR, $\omega_1$ and $\omega_2$ are the center angular frequencies of the first and second band of the DBPF, $b$ is the slope parameter, $g_i$ is the corresponding lowpass prototype element value, $FBW_r$ is the fractional bandwidth of the first or the second passband for DBPF.

The selected LC DBR structure is shown in Figure 1A. The input admittance of this LC DBR is

$$Y_B = \frac{L_1L_2C_1C_2\omega^4 - (L_1C_1 + L_2C_2)\omega^2 + 1}{j[-(C_1+C_2)L_1L_2\omega^2 + (L_1+L_2)\omega]}. \tag{4}$$

According to Equations (1) and (4), the inductances of the LC DBR are given as

$$L_1 = \frac{1}{\omega_1{}^2C_1},\ L_2 = \frac{1}{\omega_2{}^2C_2}. \tag{5}$$

Based on Equations (2) and (4), the slope parameters can be derived as

$$\begin{cases} b_{\omega_1} = \frac{\omega_1}{2}\frac{\partial}{\partial\omega}\mathrm{Im}[Y_B(\omega)]\big|_{r=1} = \omega_1C_1 \\ b_{\omega_2} = \frac{\omega_2}{2}\frac{\partial}{\partial\omega}\mathrm{Im}[Y_B(\omega)]\big|_{r=2} = \omega_2C_2. \end{cases} \tag{6}$$

Then based on Equations (3) and (6), the capacitances of the LC DBR are given as

$$C_1 = \frac{g_i}{\omega_1 FBW_1 R_S},\ C_2 = \frac{g_i}{\omega_2 FBW_2 R_S}. \tag{7}$$

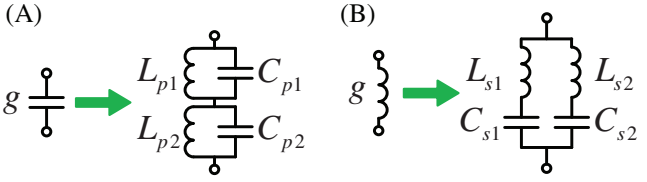


**FIGURE 2** Proposed lowpass prototype to ICBW dual-band bandpass transformation. (A) Capacitor transformation. (B) Inductor transformation

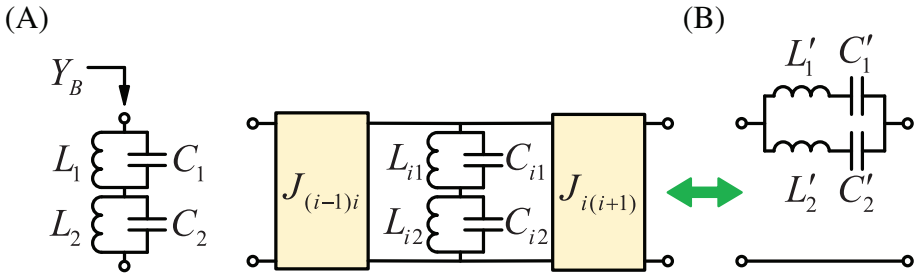


**FIGURE 1** (A) Schematics of the selected LC DBR. (B) Circuit conversion of the dual-band *J*-inverters and dual-band resonators (DBRs)

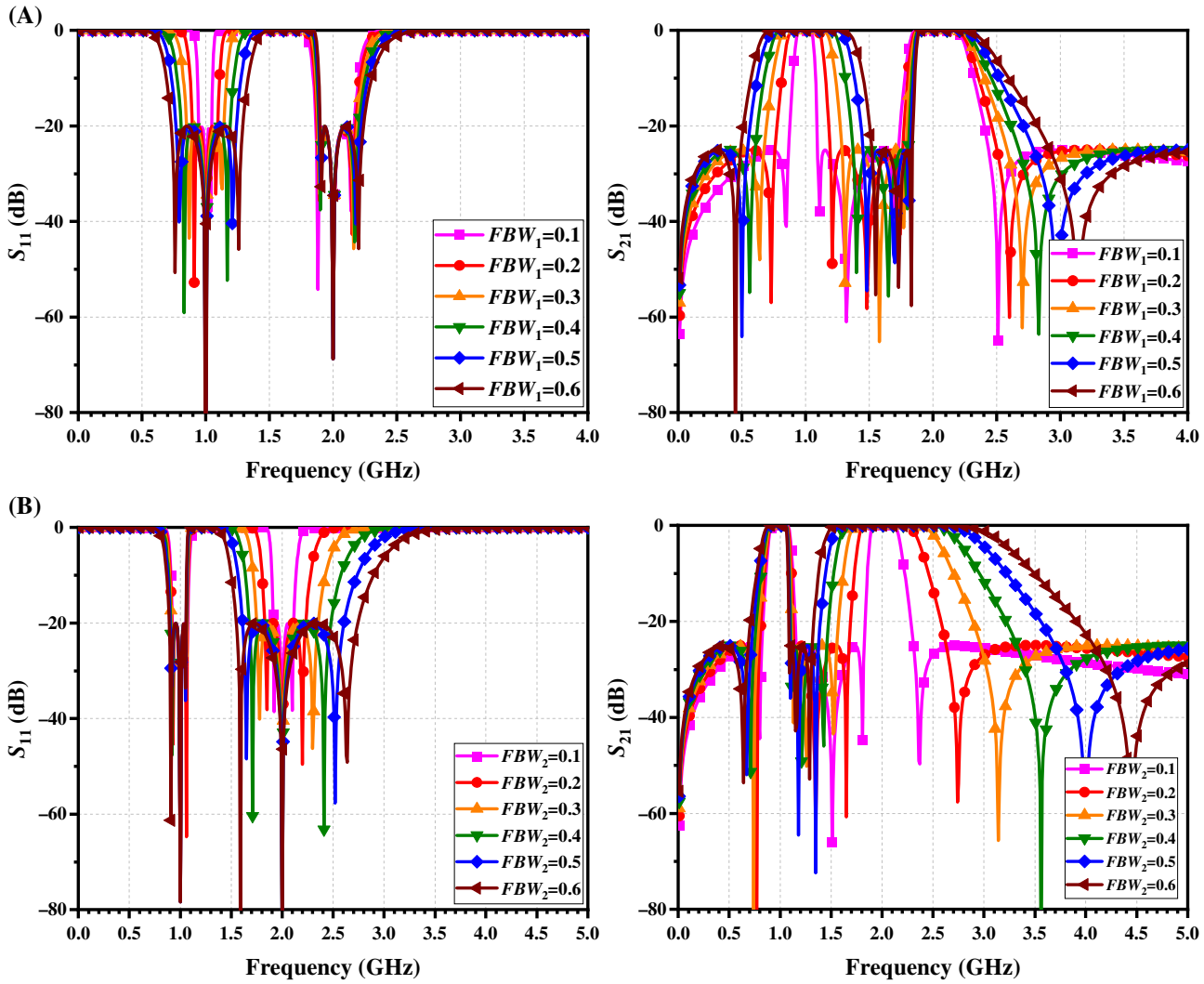


**FIGURE 3** Ideal *S*-parameters of the examples. (A) Various $FBW_1$ with the fixed value $FBW_2$. (B) Various $FBW_2$ with the fixed value $FBW_1$

**TABLE 1** Bandwidth of the different case

| Parameter *FBW* (%) | $S_{11} = -10$ dB *FBW* (%) | $S_{21} = -3$ dB *FBW* (%) |
|---|---|---|
| 10/15 | 11.0/17.5 | 14.4/21.4 |
| 20/15 | 23.0/17.5 | 28.2/21.6 |
| 30/15 | 33.0/18.0 | 41.2/22.1 |
| 40/15 | 44.0/18.5 | 53.3/22.9 |
| 50/15 | 55.0/19.5 | 64.4/24.0 |
| 60/15 | 64.0/20.5 | 74.5/25.4 |
| 15/10 | 17.0/11.5 | 21.3/14.4 |
| 15/20 | 17.0/23.5 | 21.5/28.2 |
| 15/30 | 17.0/35.0 | 22.0/41.2 |
| 15/40 | 18.0/46.5 | 22.8/53.3 |
| 15/50 | 18.0/58.0 | 23.9/64.4 |
| 15/60 | 19.0/69.5 | 25.3/74.5 |

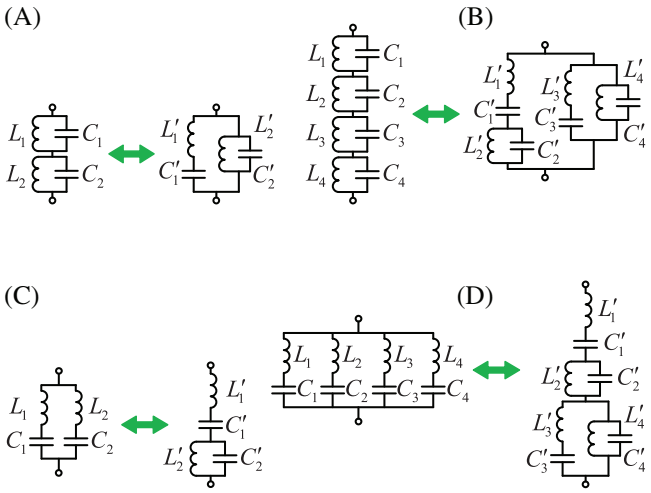


**FIGURE 4** Four common circuit equivalent conversions. (A) Type 1. (B) Type 2. (C) Type 3 (D) Type 4

The DBAI can be implemented by lumped elements, but the DBPF circuit will become complicated. The simplified circuit without DBAIs using circuit conversion is shown in Figure 1B. Similar to the above, the parameters can be expressed as

$$\begin{cases} C_1' = \dfrac{R_S g_i}{\omega_1 FBW_1}, & L_1' = \dfrac{1}{\omega_1{}^2 C_1} \\ C_2' = \dfrac{R_S g_i}{\omega_2 FBW_2}, & L_2' = \dfrac{1}{\omega_2{}^2 C_2}. \end{cases} \tag{8}$$

Therefore, based on References 2,15, a novel synthesis method of LC DBPF with independently controllable bandwidth is proposed, which is an improvement of the traditional lowpass prototype filter theory in dual-band. Figure 2 shows the proposed lowpass prototype to dual-band bandpass transformation with independently controllable bandwidth.

Values of the elements in the DBPF can be determined by

$$\begin{cases} C_{pi} = \dfrac{\Omega_c g}{FBW_i \omega_i \gamma_0} \\ L_{pi} = \dfrac{1}{\omega_i{}^2 C_{pi}} \end{cases}, g \text{ representing the capacitance} \tag{9a}$$

$$\begin{cases} L_{si} = \dfrac{\Omega_c \gamma_0 g}{FBW_i \omega_i} \\ C_{si} = \dfrac{1}{\omega_i{}^2 L_{si}} \end{cases}, g \text{ representing the inductance} \tag{9b}$$

where $\gamma_0$ is the impedance scaling factor, $\Omega_c$ is the cutoff frequency, $i = 1, 2$.

**TABLE 2** Configurations of the generalized cases

| | *Case A* | *Case B* | *Case C* |
|---|---|---|---|
| $n$ | 3 | 3 | 5 |
| $\varepsilon$ | 0.1 | 0.1 | 0.1 |
| $IL_{max}$ in stopband (dB) | 25 | 25 | 20 |
| $f_1/f_2$ (GHz) | 1/2 | 1/2 | 0.5/2 |
| $FBW_1/FBW_2$ (%) | 40/15 | 15/30 | 70/70 |

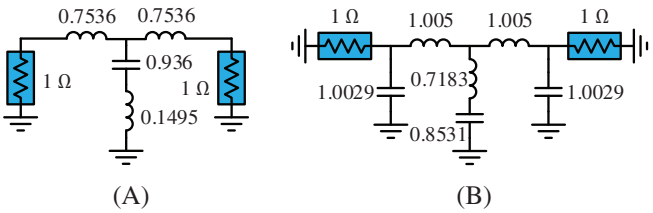


**FIGURE 5** Schematics of the lowpass prototype. (A) *Case A* and *B*. (B) *Case C*

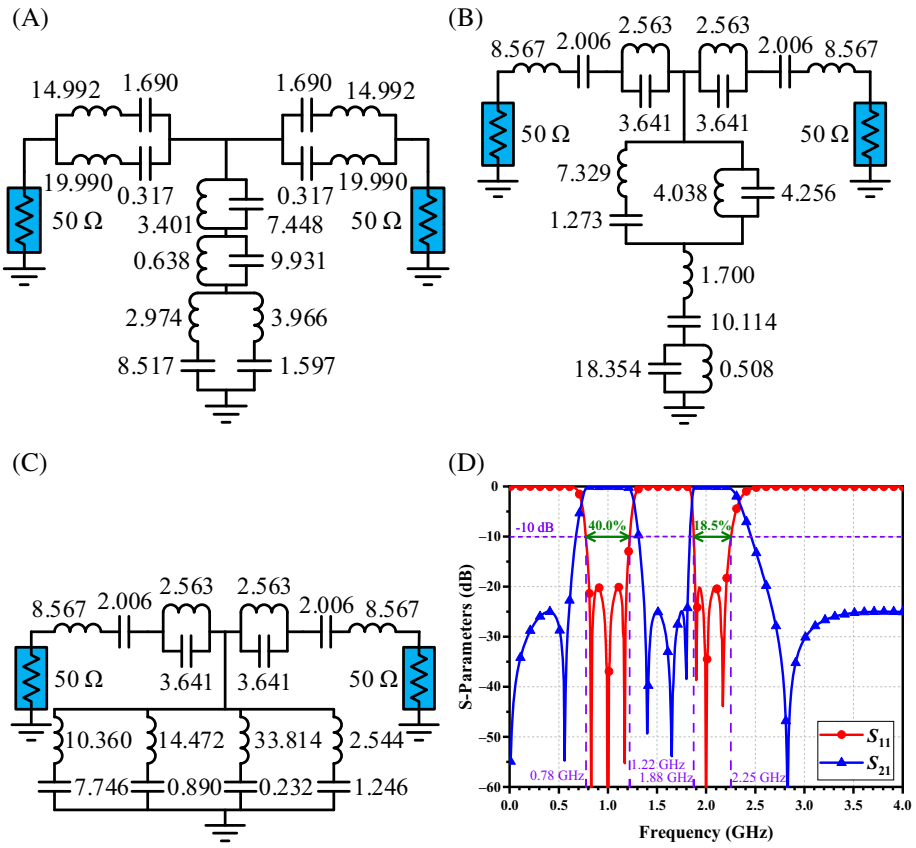


**FIGURE 6** Schematics and *S*-parameters of the *Case A*. (A) Initial DBPF. (B) All converted DBPF. (C) Final converted DBPF. (D) Ideal *S*-parameters

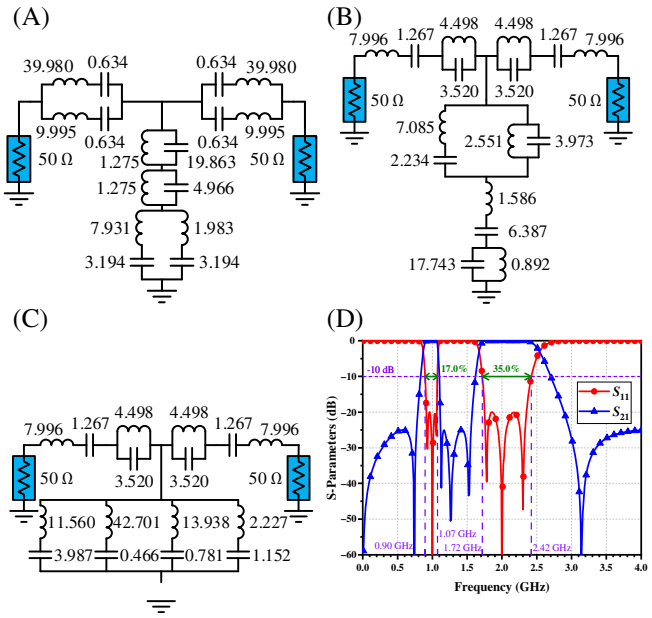


**FIGURE 7** Schematics and *S*-parameters of the *Case B*. (A) Initial DBPF. (B) All converted DBPF. (C) Final converted DBPF. (D) Ideal *S*-parameters

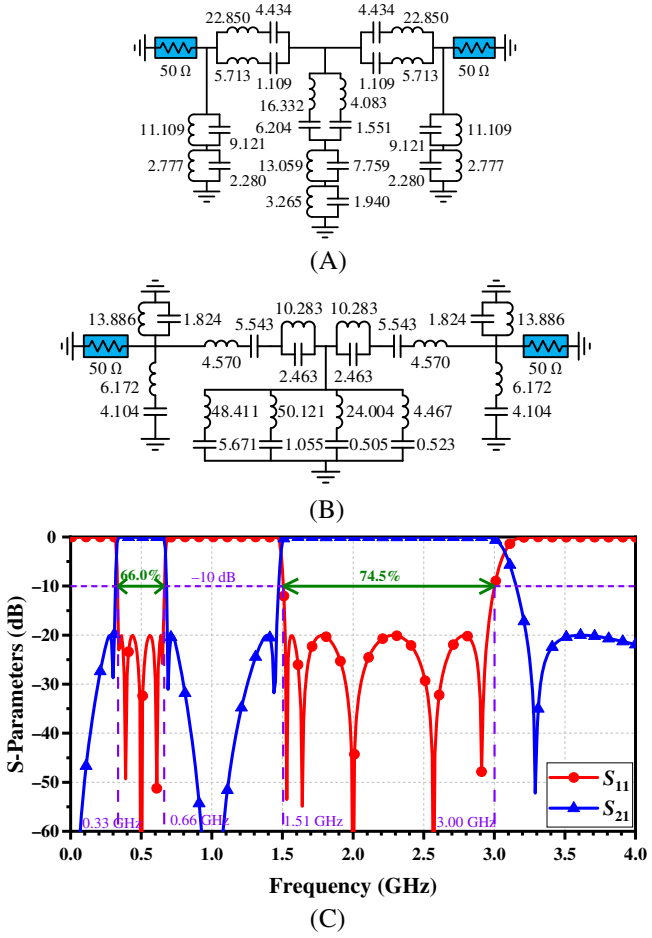


**FIGURE 8** Schematics and *S*-parameters of the *Case C*. (A) Initial DBPF. (B) Final converted DBPF. (C) Ideal *S*-parameters

Two examples are given to verify the independently controllable bandwidth function of DBPF. Both examples are third-order quasi-elliptic DBPFs with $f_1$ at 1 GHz, $f_2$ at 2 GHz, $\varepsilon = 0.1$, $IL_{\max}$ in stopband = 25 dB. Figure 3A, B show the ideal *S*-parameters of the DBPF for various $FBW_1$ with the fixed value $FBW_2 = 15\%$ (Example 1) and the *S*-parameters of the DBPF for various $FBW_2$ with the fixed value $FBW_1 = 15\%$ (Example 2), respectively.

Table 1 shows the bandwidth of the different cases. In Example 1, when $FBW_1$ increases, the bandwidth of the second passband slightly increases. A slight deviation of the fixed bandwidth can be allowed.

In filter design, circuit equivalent conversion is often used which can be easier implemented. Figure 4 shows the four common circuit equivalent conversions. The equivalent conversion of the circuit is based on the equal input impedance. After dual-band frequency transformation based on (9), the initial DBPF circuit can be converted by the four-parameter circuit conversions in Figure 4A,C. The eight-parameter circuit conversion in Figure 4B can reduce the sensitivity of the performance to lumped elements values significantly by utilizing relatively large inductances, as explained in Reference 12. Whether or not the parameter values are simple to implement determines which conversion method to choose.

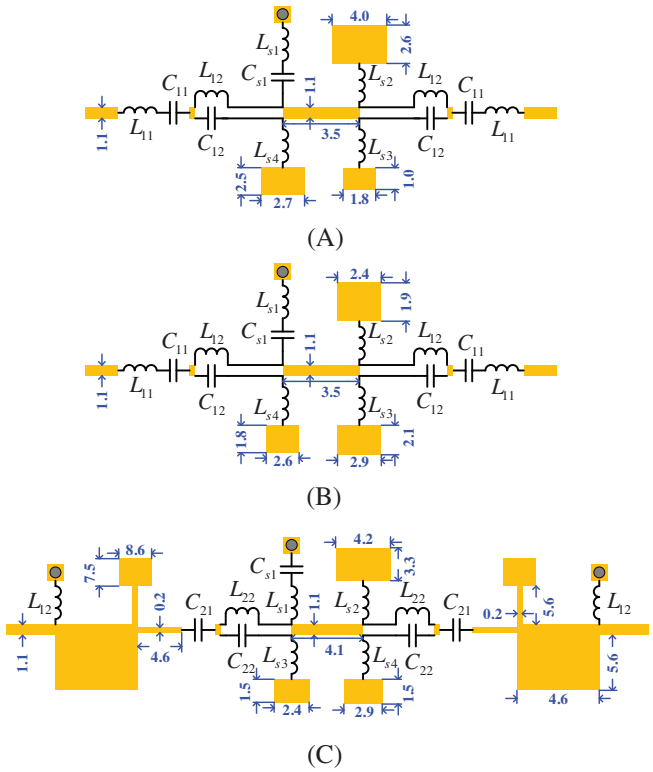


**FIGURE 9** Layout of the manufactured DBPF (unit: mm). (A) *Case A*. (B) *Case B*. (C) *Case C*

**TABLE 3** Parameter values of the three cases

| | *Case A* | *Case B* | *Case C* |
|---|---|---|---|
| $L$ (nH) | $L_{11} = 4.8$ | $L_{11} = 6.2$ | $L_{12} = 12.0$ |
| | $L_{12} = 3.0$ | $L_{12} = 4.1$ | $L_{22} = 10.0$ |
| | $L_{s1} = 10.0$ | $L_{s1} = 12.0$ | $L_{s1} = 47.0$ |
| | $L_{s2} = 11.0$ | $L_{s2} = 33.0$ | $L_{s2} = 33.0$ |
| | $L_{s3} = 27.0$ | $L_{s3} = 18.0$ | $L_{s3} = 20.0$ |
| | $L_{s4} = 3.5$ | $L_{s4} = 5.0$ | $L_{s4} = 4.2$ |
| $C$ (pF) | $C_{11} = 2.4$ | $C_{11} = 1.4$ | $C_{21} = 7.0$ |
| | $C_{12} = 4.2$ | $C_{12} = 3.7$ | $C_{22} = 2.3$ |
| | $C_{s1} = 7.0$ | $C_{s1} = 3.4$ | $C_{s1} = 6.0$ |

Finally, the overall design procedure for the proposed DBPF with independently controllable bandwidth can be summarized as follows.

1. *Step 1*: Given the filter order $n$, the passband ripple level $\varepsilon$, and $IL_{\max}$ in stopband. Get the elements of the lowpass prototype.
2. *Step 2*: Given $f_1$, $f_2$, $FBW_1$, and $FBW_2$. Calculate the LC values according to Equation (9).
3. *Step 3*: Convert the initial DBPF to all-converted DBPF according to four-parameter circuit equivalent conversions in Figure 4A,C.
4. *Step 4*: Convert all-converted DBPF according to eight-parameter circuit equivalent conversions in

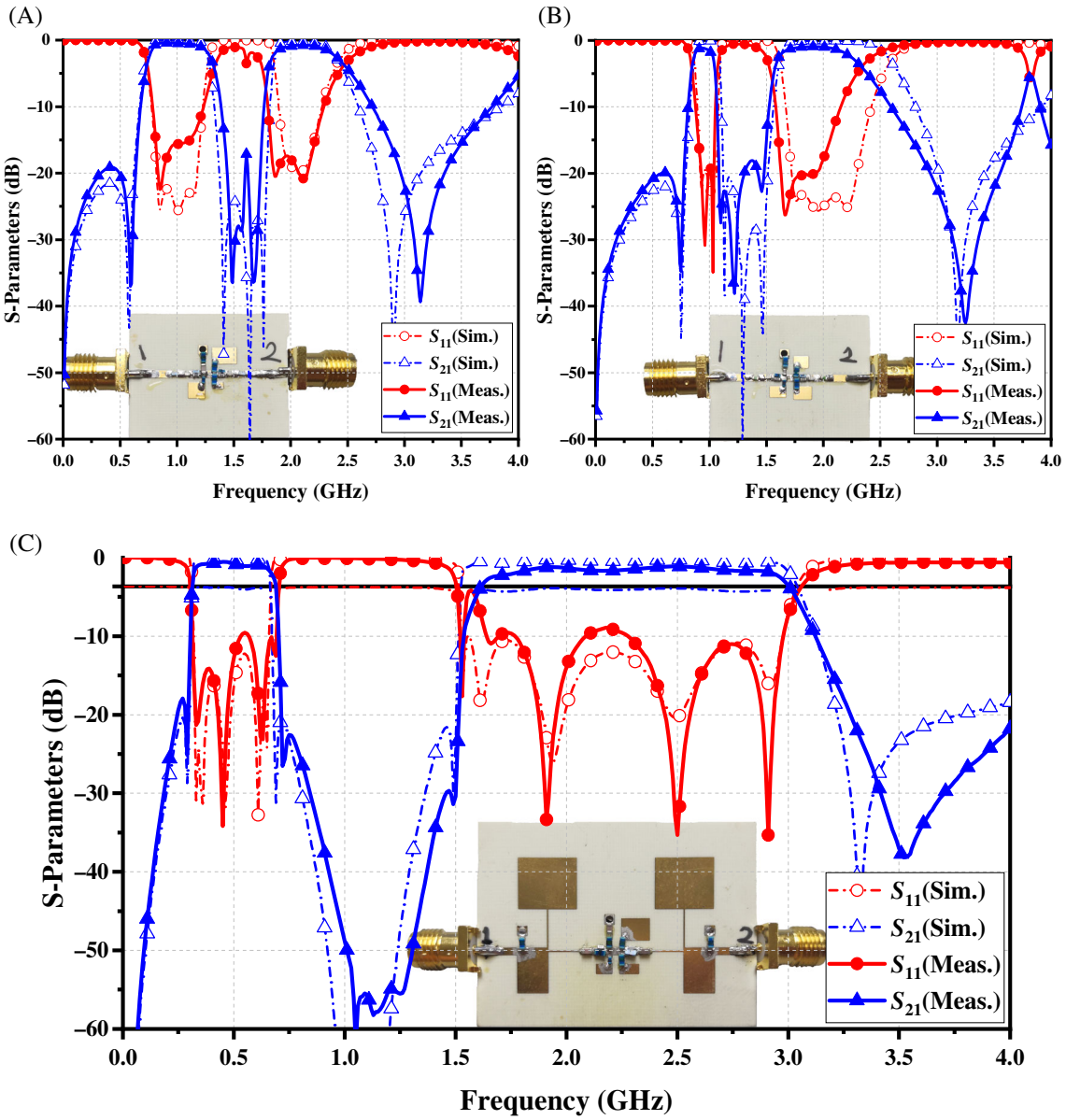


**FIGURE 10** Simulated and measured $S$-parameters of the presented DBPF. (A) *Case A*. (B) *Case B*. (C) *Case C*

**TABLE 4** Comparison with previous dual-band BPFs

| Refs. | $f_1/f_2$ (GHz) | Frequency ratio | 3-dB | RL in passband (dB) | IL in passband (dB) | TZs | Order | Size ($\lambda_g \times \lambda_g$) |
|---|---|---|---|---|---|---|---|---|
| 2 | 1.8/2.4 | 1.3 | 2.8/2.8 | 17/17 | 3/4 | 3 | 2/2 | 0.75 × 0.75 |
| 6 | 0.71/1.37 | 1.9 | 41.1/19.0 | 13/15 | 0.6/1.0 | 8 | - | 0.33 × 0.05 |
| 7 | 2.4/5 | 2.1 | 14.6/5.8 | 10/10 | 0.9/1.6 | 6 | - | 0.58 × 0.26 |
| 12 I | 1/2 | 2 | 8.5/9 | 10/10 | 1.0/0.7 | 5 | 3/3 | 0.08 × 0.08 |
| 13 Third | 0.62/1.41 | 2.3 | 28.2/18.2 | 20/10 | 0.9/1.7 | 2 | 3/3 | 0.47 × 0.47 |
| 14 II | 1/2.2 | 2.2 | 43/19.5 | 18/18 | 0.4/0.9 | 3 | 3/3 | 0.38 × 0.57 |
| *Case A* | 1/2 | 2 | 55/30 | 15/17 | 0.5/0.8 | 5 | 3/3 | 0.05 × 0.08 |
| *Case B* | 1/2 | 2 | 18/34 | 19/18 | 1.2/1.0 | 5 | 3/3 | 0.05 × 0.08 |
| *Case C* | 0.5/2 | 4 | 72/67 | 9/8 | 1.0/2.1 | 5 | 5/5 | 0.06 × 0.09 |

*Note*: $\lambda_g$: Guide wavelength on the substrate at the center frequency of the first passband. All values are measured results.
Abbreviations: FBW, fractional bandwidth; IL, insertion loss; RL, return loss; TZ, transmission zero.

Figure 4B,D. Compare the all-converted DBPF and the DBPF in this step to choose the one that is easy to realize as the final circuit.

## 3 | DESIGN EXAMPLES

Three design examples of DBPFs (*Case A*, *B*, and *C*) are given. The configurations of the cases are listed in Table 2. The generalized quasi-elliptic lowpass prototype are employed, which are shown in Figure 5. The conversion procedures of the circuit with all the values and the ideal *S*-parameters are shown in Figures 6–8. The unit of capacitance is pF, and the unit of inductance is nH. In order to implement easily, some shunt capacitors are approximated by open-stubs, some shunt inductors are approximated by short-stubs.[16]

All the cases are fabricated and measured on Rogers4350B substrate ($\varepsilon_r = 3.66$, $\delta = 0.0037$) with a thickness of 0.508 mm. Three layouts of the fabricated DBPF are shown in Figure 9. Lumped components values are described in Table 3. The MuRata lumped components are used. The MuRata's GRM15 capacitors and LQG15, LQW15 inductors are used.

The measured results are obtained by the vector network analyzer of Rohde & Schwarz ZVA8. The EM simulated and measured results of the three cases, as well as the photographs of the fabricated circuits, are shown in Figure 10.

In *Case A*, the measured 3-dB fractional bandwidths are 55% (0.70–1.30 GHz) and 30% (1.83–2.43 GHz) with the designated center frequency of 1 and 2 GHz. Within the two passbands, the measured insertion losses are below 0.5 and 0.8 dB. The return loss is greater than 15 dB from 0.81 to 1.11 GHz in the first passband and greater than 17 dB from 1.84 to 2.18 GHz in the second passband. In *Case B*, the measured 3-dB fractional bandwidths are 18% (0.86–1.04 GHz) and 34% (1.60–2.28 GHz) with the designated center frequency of 1 and 2 GHz. Within the two passbands, the measured insertion losses are below 1.2 and 1.0 dB. The return loss is greater than 19 dB from 0.93 to 1.04 GHz in the first passband and greater than 18 dB from 1.63 to 1.99 GHz in the second passband. In *Case C*, the measured 3-dB fractional bandwidths are 72% (0.32–0.68 GHz) and 67% (1.64–2.98 GHz) with the designated center frequency of 0.5 and 2 GHz. Within the two passbands, the measured insertion losses are below 1.0 and 2.1 dB. The return loss is greater than 9 dB from 0.32 to 0.69 GHz in the first passband and greater than 8 dB from 1.63 to 2.99 GHz in the second passband. The deviation between the measured and ideal performance is mainly attributed to the conductor loss, the connection lines between the lumped components, and the low-quality factor of the relatively large inductances.

Overall, good agreement between the simulated and measured results is observed. The comparisons with the reported DBPFs are listed in Table 4 to highlight the advantages of the proposed compact LC DBPFs.

## 4 | CONCLUSION

In this brief, a novel synthesis method of compact LC DBPFs with independently controllable bandwidth is presented. The method is based on dual-band frequency transformation and circuit conversions. Three cases of DBPF with different frequency ratios, different bandwidths,

and different orders are designed, manufactured, and measured, which reveals the validity of the proposed design theory. The proposed lumped-element DBPF exhibits the advantages including two passbands with independently controllable bandwidth, arbitrary frequency ratio, large range of FBW, availability for different lowpass prototypes, and compact dimensions below 6 GHz. It is predictable that the presented DBPF design methodology can be applied to design and implement the multi-band filter and the proposed method will be widely used in dual−/multi-band RF wireless circuits and systems.

## ACKNOWLEDGMENTS

This work was supported by National Natural Science Foundations of China (Nos. U20A20203, U21A20510, and 61971052), the Fundamental Research Funds for the Central Universities (2021XD-A07-1), and Key Research and Development Project of Guangdong Province (2020B0101080001).

## DATA AVAILABILITY STATEMENT

The data that support the findings of this study are available from the corresponding author upon reasonable request.

## ORCID

*Zhuoyin Chen* https://orcid.org/0000-0002-0059-9303
*Yongle Wu* https://orcid.org/0000-0002-3269-7143
*Weimin Wang* https://orcid.org/0000-0003-3110-3259

## REFERENCES

1. Tsai L-C, Hsue C-W. Dual-band bandpass filters using equal-length coupled-serial-shunted lines and Z-transform technique. *IEEE Trans Microw Theory Tech*. 2004;52(4):1111-1117.
2. Guan X, Ma Z, Cai P, Kobayashi Y, Anada T, Hagiwara G. Synthesis of dual-band bandpass filters using successive frequency transformations and circuit conversions. *IEEE Microw Wireless Compon Lett*. 2006;16(3):110-112.
3. Lee J, Sarabandi K. A synthesis method for dual-passband microwave filters. *IEEE Trans Microw Theory Tech*. 2007;55(6):1163-1170.
4. Chen X, Zhang L, Xu C, Zheng Z, Jiang X. Dual-band filter synthesis based on two low-pass prototypes. *IEEE Microw Wireless Compon Lett*. 2017;27(10):903-905.
5. Liu A, Huang T, Wu R. A dual wideband filter design using frequency mapping and stepped-impedance resonators. *IEEE Trans Microw Theory Tech*. 2008;56(12):2921-2929.
6. Wu Y, Cui L, Zhuang Z, Wang W, Liu Y. A simple planar dual-band bandpass filter with multiple transmission poles and zeros. *IEEE Trans Circuits Syst II Exp Briefs*. 2018;65(1):56-60.
7. Shi L-F, Zhao L, Zhang X-L. Dual-band filter with high selectivity and wide stopband rejection. *Int J RF Microw Comput-Aided Eng*. 2020;30(11):e22403. doi: 10.1002/mmce.22403
8. Sun X, Tan EL. Dual-band filter design with pole-zero distribution in the complex frequency plane. Paper presented at: 2016 IEEE MTT-S International Microwave Symposium (IMS); May 22-27, 2016; San Francisco, CA:1-4.
9. Mao S, Wu M. Design of artificial lumped-element coplanar waveguide filters with controllable dual-passband responses. *IEEE Trans Microw Theory Tech*. 2008;56(7):1684-1692.
10. Liu Y, Chen Y, Miao X, Cui C, Tang Y. Synthesis method of lumped dual–band filters with controllable bandwidths. *Int J RF Microw Comput-Aided Eng*. 2015;25(1):75-80.
11. Joshi H, Chappell WJ. Dual-band lumped-element bandpass filter. *IEEE Trans Microw Theory Tech*. 2006;54(12):4169-4177.
12. Dai X, Yang Q, Du H, Guo C, Zhang A. Direct synthesis method for dual-band bandpass filters with wide fractional bandwidth range and center frequency ratio. *IEEE Trans Circuits Syst II Exp Briefs*. 2021;68(8):2755-2759.
13. Zhang R, Luo S, Zhu L. Synthesis and design of asymmetrical dual-band bandpass filters with modified Richard's transformation. *IET Microw Antennas Propag*. 2016;10(12):1352-1362.
14. Chen W, Wu Y, Wang W, Xu K, Shi J. Synthesis design on wideband single-ended and differential dual-band filtering impedance transformer. *IEEE Trans Circuits Syst II Exp Briefs*. 2021;68(3):913-917.
15. Wu Y, Zhuang Z, Yan G, Liu Y, Ghassemlooy Z. Generalized dual-band unequal filtering power divider with independently controllable bandwidth. *IEEE Trans Microw Theory Tech*. 2017;65(10):3838-3848.
16. Hong J-S. *Microstrip Filters for RF/Microwave Applications*. 2nd ed. Wiley; 2011.

**How to cite this article:** Chen Z, Wu Y, Wang W. Synthesis of lumped-element dual-band bandpass filters with independently controllable bandwidth. *Int J RF Microw Comput Aided Eng*. 2022;32(5):e23076. doi:10.1002/mmce.23076